

VIBRATIONAL ANALYSIS OF DOUBLE-WALLED CARBON NANOTUBES BASED ON THE NONLOCAL DONNELL SHELL THEORY VIA A NEW NUMERICAL APPROACH*

R. ANSARI¹, H. ROUHI^{2**} AND B. ARASH³

^{1,2}Dept. of Mechanical Engineering, University of Guilan, P.O. Box 3756, Rasht, I. R. of Iran
Email: rouhi.hessam@gmail.com

³Dept. of Mechanical and Manufacturing Engineering, University of Manitoba,
Winnipeg, Manitoba, Canada, R3T 5V6

Abstract– This article describes an investigation into the free vibration of double-walled carbon nanotubes (DWCNTs) using a nonlocal elastic shell model. Eringen's nonlocal elasticity is implemented to incorporate the scale effect into the Donnell shell model. Also, the van der Waals interaction between the inner and outer nanotubes is taken into account. A new numerical solution method from incorporating the radial point interpolation approximation within the framework of the generalized differential quadrature (GDQ) method is developed to solve the problem. DWCNTs with arbitrary layerwise boundary conditions are considered in this paper. It is shown that applying the local Donnell shell model leads to overestimated results and one must recourse to the nonlocal version to reduce the relative error. Also, this work reveals that in contrast to the beam model, the present nonlocal elastic shell model is capable of predicting some new non-coaxial inter-tube resonances in studying the vibrational response of DWCNTs.

Keywords– Double-walled carbon nanotube, radial point interpolation method, differential quadrature method, layerwise boundary conditions

1. INTRODUCTION

Ever since carbon nanotubes (CNTs) were discovered by Iijima at the NEC laboratory in Tsukuba, Japan [1], extensive theoretical and experimental studies have been conducted on these novel materials [2]. DWCNTs as the special cases of multi-walled CNTs can be made in quantitative amounts from the chains of fullerenes generated inside single-walled CNTs [3]. In recent years, DWCNTs have drawn a great deal of attention from the scientific community due to their amazing mechanical, optical and chemical properties.

It is generally accepted that atomistic modeling of nanostructures is very time consuming. Accordingly, it is advantageous to develop continuum models for the analysis of nanostructures due to their computational efficiency. Since the conventional continuum mechanics is scale free, great attempts have recently been devoted to the enhancement of classical continuum models in order to better accommodate the results from molecular dynamics (MD) simulations. In the most commonly used size-dependant continuum theory, nonlocal continuum theory, developed by Eringen [4, 5], the scale effect is simply introduced into the constitutive equations as a material parameter.

Recently, the vibration analysis of CNTs has been the subject of numerous studies based on both local and nonlocal models using beam and shell theories [6-17]. For example, Ansari et al. [9] studied the free vibration of DWCNTs based on the nonlocal Donnell shell model using an analytical solution method. They also employed the MD simulations in order to calibrate the nonlocal parameter used in their nonlocal model.

*Received by the editors July 29, 2012; Accepted December 2, 2012.

**Corresponding author

For a DWCNT, different combinations of layerwise boundary conditions can be considered. In this respect, Xu et al. [7] stated that: “The relevance of the existing model in which both tubes have the same boundary conditions for the vibration of double-walled CNTs is questionable”. Therefore, developing powerful numerical solution methods capable of treating layerwise boundary conditions in a DWCNT can play an important role in the advancement of computational nanomechanics. Hence, the main aim of the current work is to extend the study reported in [9] on DWCNTs with the same boundary conditions for the inner and outer tubes to DWCNTs with layerwise boundary conditions. To this end, a novel numerical method termed as RPIDQ is developed within the framework of hybrid radial point interpolation [18] and differential quadrature method [19]. The effectiveness of the present model is assessed by MD simulation as a benchmark of good accuracy. In addition, this study provides a comparison between the beam and shell models in predicting the frequencies of DWCNTs. To accomplish this goal, an explicit formula is also derived for the nonlocal frequencies of DWCNTs based on the beam model. Some new inter-tube resonant frequencies and the related non-coaxial vibrational modes are identified in this work as a result of incorporating circumferential modes into the shell model.

2. MODELING

In the theory of nonlocal elasticity, unlike the conventional continuum mechanics, the stress at a point is considered to be a functional of the strain field at all points in the body. To bring the nonlocality into formulation, the Eringen nonlocal constitutive equation is employed as [5]

$$(1 - (e_0 a)^2 \nabla^2) \sigma = t \tag{1}$$

here $e_0 a$ stands for the nonlocal parameter which leads to consideration of the scale effect and ∇^2 is the Laplacian operator; t is the macroscopic stress tensor at a point. The stress tensor is related to strain by generalized Hooke’s law as

$$t = S : \epsilon \tag{2}$$

where S is the fourth order elasticity tensor and ‘:’ denotes the double dot product. Hooke’s law for the stress and strain relation is given by

$$\begin{Bmatrix} \sigma_{xx} \\ \sigma_{\theta\theta} \\ \sigma_{x\theta} \\ \sigma_{\theta z} \\ \sigma_{xz} \end{Bmatrix} - (e_0 a)^2 \nabla^2 \begin{Bmatrix} \sigma_{xx} \\ \sigma_{\theta\theta} \\ \sigma_{x\theta} \\ \sigma_{\theta z} \\ \sigma_{xz} \end{Bmatrix} = \begin{bmatrix} \frac{E}{1-\nu^2} & \frac{\nu E}{1-\nu^2} & 0 & 0 & 0 \\ \frac{\nu E}{1-\nu^2} & \frac{E}{1-\nu^2} & 0 & 0 & 0 \\ 0 & 0 & G & 0 & 0 \\ 0 & 0 & 0 & G & 0 \\ 0 & 0 & 0 & 0 & G \end{bmatrix} \begin{Bmatrix} \epsilon_{xx} \\ \epsilon_{\theta\theta} \\ \gamma_{x\theta} \\ \gamma_{\theta z} \\ \gamma_{xz} \end{Bmatrix} \tag{3}$$

where E, G and ν are Young’s modulus, shear modulus and Poisson’s ratio of the material, respectively. Consider an elastic cylindrical shell with radius R , length L and thickness h for each tube of a DWCNT (see Fig. 1). There are different theories for cylindrical shells such as Flugge’s theory [20, 21] or Donnell’s theory [22]. In Donnell’s shell theory, the shear and rotary inertia effects are taken into account. Thus, it seems to be suitable for the vibration analysis of cylindrical shells. Also, it is frequently used for the analysis of CNTs due to the relatively accurate results in spite of its theoretical simplicity. Based on the Donnell shell theory, the three-dimensional displacement components u_x, u_y and u_z in the x, θ and z directions respectively, as shown in Fig. 1, are assumed to be

$$u_x(x, \theta, z, t) = u(x, \theta, t) + z\psi_x(x, \theta, t) \tag{4a}$$

$$u_y(x, \theta, z, t) = v(x, \theta, t) + z\psi_\theta(x, \theta, t) \tag{4b}$$

$$u_z(x, \theta, z, t) = w(x, \theta, z, t) \tag{4c}$$

where u, v, w are mid-surface displacements and ψ_x, ψ_θ are mid-surface rotations. The mid-surface strains and curvature changes are given by

$$\begin{aligned} \varepsilon_{0x} = \frac{\partial u}{\partial x}, \quad \varepsilon_{0\theta} = \frac{1}{R} \frac{\partial v}{\partial \theta} + \frac{w}{R}, \quad \gamma_{0x\theta} = \frac{\partial v}{\partial x} + \frac{1}{R} \frac{\partial u}{\partial \theta}, \quad k_x = \frac{\partial \psi_x}{\partial x}, \quad k_\theta = \frac{1}{R} \frac{\partial \psi_\theta}{\partial \theta}, \\ k_{x\theta} = \frac{\partial \psi_\theta}{\partial x} + \frac{1}{R} \frac{\partial \psi_x}{\partial \theta}, \quad \gamma_{0xz} = \frac{\partial w}{\partial x} + \psi_x, \quad \gamma_{\theta z} = \frac{1}{R} \frac{\partial w}{\partial \theta} - \frac{v}{R} + \psi_\theta \end{aligned} \tag{5}$$

The strains at any point in the shell thickness can then be written in terms of mid-surface strains and curvature changes as

$$\varepsilon_x = \varepsilon_{0x} + zk_x \tag{6a}$$

$$\varepsilon_\theta = \varepsilon_{0\theta} + zk_\theta \tag{6b}$$

$$\gamma_{x\theta} = \gamma_{0x\theta} + zk_{x\theta} \tag{6c}$$

$$\gamma_{xz} = \gamma_{0xz} \tag{6d}$$

$$\gamma_{\theta z} = \gamma_{0\theta z} + z(\psi_\theta/R) \tag{6e}$$

Using Eqs. (3) to (6) the stress and moment resultants can be given as follows

$$N_{xx} = \int_{-h/2}^{h/2} \sigma_{xx} dz \quad i. e. \quad N_{xx} - (e_0 a)^2 \nabla^2 N_{xx} = \frac{Eh}{1-\nu^2} \frac{\partial u}{\partial x} + \frac{\nu Eh}{1-\nu^2} \left(\frac{1}{R} \frac{\partial v}{\partial \theta} + \frac{w}{R} \right) \tag{7a}$$

$$N_{\theta\theta} = \int_{-h/2}^{h/2} \sigma_{\theta\theta} dz \quad i. e. \quad N_{\theta\theta} - (e_0 a)^2 \nabla^2 N_{\theta\theta} = \frac{\nu Eh}{1-\nu^2} \frac{\partial u}{\partial x} + \frac{Eh}{1-\nu^2} \left(\frac{1}{R} \frac{\partial v}{\partial \theta} + \frac{w}{R} \right) \tag{7b}$$

$$N_{x\theta} = \int_{-h/2}^{h/2} \sigma_{x\theta} dz \quad i. e. \quad N_{x\theta} - (e_0 a)^2 \nabla^2 N_{x\theta} = Gh \left(\frac{\partial v}{\partial x} + \frac{1}{R} \frac{\partial u}{\partial \theta} \right) \tag{7c}$$

$$M_{xx} = \int_{-h/2}^{h/2} z \sigma_{xx} dz \quad i. e. \quad M_{xx} - (e_0 a)^2 \nabla^2 M_{xx} = D \left(\frac{\partial \psi_x}{\partial x} + \frac{\nu}{R} \frac{\partial \psi_\theta}{\partial \theta} \right) \tag{7d}$$

$$M_{\theta\theta} = \int_{-h/2}^{h/2} z \sigma_{\theta\theta} dz \quad i. e. \quad M_{\theta\theta} - (e_0 a)^2 \nabla^2 M_{\theta\theta} = D \left(\frac{1}{R} \frac{\partial \psi_\theta}{\partial \theta} + \nu \frac{\partial \psi_x}{\partial x} \right) \tag{7e}$$

$$M_{x\theta} = \int_{-h/2}^{h/2} z \sigma_{x\theta} dz \quad i. e. \quad M_{x\theta} - (e_0 a)^2 \nabla^2 M_{x\theta} = \frac{1}{2} D (1-\nu) \left(\frac{\partial \psi_\theta}{\partial x} + \frac{1}{R} \frac{\partial \psi_x}{\partial \theta} \right) \tag{7f}$$

$$Q_{xx} = \int_{-h/2}^{h/2} \sigma_{xz} dz \quad i. e. \quad Q_{xx} - (e_0 a)^2 \nabla^2 Q_{xx} = Gh \left(\frac{\partial w}{\partial x} + \psi_x \right) \tag{7g}$$

$$Q_{\theta\theta} = \int_{-h/2}^{h/2} \sigma_{\theta z} dz \quad i. e. \quad Q_{\theta\theta} - (e_0 a)^2 \nabla^2 Q_{\theta\theta} = Gh \left(\frac{1}{R} \frac{\partial w}{\partial \theta} - \frac{v}{R} + \psi_\theta \right) \tag{7h}$$

where D is the bending rigidity. The governing equations are

$$\frac{\partial N_{xx}}{\partial x} + \frac{1}{R} \frac{\partial N_{x\theta}}{\partial \theta} = I_1 \ddot{u} + I_2 \ddot{\psi}_x \tag{8a}$$

$$\frac{\partial N_{x\theta}}{\partial x} + \frac{1}{R} \frac{\partial N_{\theta\theta}}{\partial \theta} + \frac{Q_{\theta\theta}}{R} = I_1 \dot{v} + I_2 \ddot{\psi}_\theta \tag{8b}$$

$$\frac{\partial Q_{xx}}{\partial x} + \frac{1}{R} \frac{\partial Q_{\theta\theta}}{\partial \theta} - \frac{N_{\theta\theta}}{R} + p = I_1 \ddot{w} \tag{8c}$$

$$\frac{\partial M_{xx}}{\partial x} + \frac{1}{R} \frac{\partial M_{x\theta}}{\partial \theta} - Q_{xx} = I_2 \ddot{u} + I_3 \ddot{\psi}_x \tag{8d}$$

$$\frac{\partial M_{x\theta}}{\partial x} + \frac{1}{R} \frac{\partial M_{\theta\theta}}{\partial \theta} - Q_{\theta\theta} = I_2 \dot{v} + I_3 \ddot{\psi}_\theta \tag{8e}$$

in which $[I_1, I_2, I_3] = \int_{-\frac{h}{2}}^{\frac{h}{2}} \rho [1, z, z^2] dz$ are the inertia terms. Also, p denotes the pressure exerted on the i th tube through the vdW interaction forces [9]. Eqs. (8) are multiplied by $(1 - (e_0 a)^2 \nabla^2)$. The left hand side of the resulting equations is given by Eqs. (7). Thus, for the i th tube of a DWCNT, by the use of Eqs. (7), Eqs. (8) can be stated in terms of the five field variables $(u^{(i)}, v^{(i)}, w^{(i)}, \psi_x^{(i)}, \psi_\theta^{(i)}, (i = 1, 2))$ as

$$l_{11}^{(i)} u^{(i)} + l_{12}^{(i)} v^{(i)} + l_{13}^{(i)} w^{(i)} + l_{14}^{(i)} \psi_x^{(i)} + l_{15}^{(i)} \psi_\theta^{(i)} \tag{9a}$$

$$= I_1 \ddot{u}^{(i)} + I_2 \ddot{\psi}_x^{(i)} - (e_0 a)^2 \left[I_1 \left(\ddot{u}_{xx}^{(i)} + \frac{1}{R_i^2} \ddot{u}_{\theta\theta}^{(i)} \right) + I_2 \left(\ddot{\psi}_{x_{xx}}^{(i)} + \frac{1}{R_i^2} \ddot{\psi}_{x_{\theta\theta}}^{(i)} \right) \right]$$

$$l_{21}^{(i)} u^{(i)} + l_{22}^{(i)} v^{(i)} + l_{23}^{(i)} w^{(i)} + l_{24}^{(i)} \psi_x^{(i)} + l_{25}^{(i)} \psi_\theta^{(i)} \tag{9b}$$

$$= I_1 \dot{v}^{(i)} + I_2 \ddot{\psi}_\theta^{(i)} - (e_0 a)^2 \left[I_1 \left(\dot{v}_{xx}^{(i)} + \frac{1}{R_i^2} \dot{v}_{\theta\theta}^{(i)} \right) + I_2 \left(\ddot{\psi}_{\theta_{xx}}^{(i)} + \frac{1}{R_i^2} \ddot{\psi}_{\theta_{\theta\theta}}^{(i)} \right) \right]$$

$$l_{31}^{(i)} u^{(i)} + l_{32}^{(i)} v^{(i)} + l_{33}^{(i)} w^{(i)} + l_{34}^{(i)} \psi_x^{(i)} + l_{35}^{(i)} \psi_\theta^{(i)} \tag{9c}$$

$$= I_1 \ddot{w}^{(i)} + w^{(i)} \sum_{\substack{j=1 \\ j \neq i}}^N c_{ij} - \sum_{\substack{j=1 \\ j \neq i}}^N c_{ij} w^{(j)}$$

$$- (e_0 a)^2 \left[I_1 \left(\ddot{w}_{xx}^{(i)} + \frac{1}{R_i^2} \ddot{w}_{\theta\theta}^{(i)} \right) + \left(w_{xx}^{(i)} + \frac{1}{R_i^2} w_{\theta\theta}^{(i)} \right) \sum_{j=2}^N c_{ij} - \sum_{j=2}^N c_{ij} \left(w_{xx}^{(j)} + \frac{1}{R_i^2} w_{\theta\theta}^{(j)} \right) \right]$$

$$l_{41}^{(i)} u^{(i)} + l_{42}^{(i)} v^{(i)} + l_{43}^{(i)} w^{(i)} + l_{44}^{(i)} \psi_x^{(i)} + l_{45}^{(i)} \psi_\theta^{(i)} \tag{9d}$$

$$= I_2 \ddot{u}^{(i)} + I_3 \ddot{\psi}_x^{(i)} - (e_0 a)^2 \left[I_2 \left(\ddot{u}_{xx}^{(i)} + \frac{1}{R_i^2} \ddot{u}_{\theta\theta}^{(i)} \right) + I_3 \left(\ddot{\psi}_{x_{xx}}^{(i)} + \frac{1}{R_i^2} \ddot{\psi}_{x_{\theta\theta}}^{(i)} \right) \right]$$

$$l_{51}^{(i)} u^{(i)} + l_{52}^{(i)} v^{(i)} + l_{53}^{(i)} w^{(i)} + l_{54}^{(i)} \psi_x^{(i)} + l_{55}^{(i)} \psi_\theta^{(i)} \tag{9e}$$

$$= I_2 \dot{v}^{(i)} + I_3 \ddot{\psi}_\theta^{(i)} - (e_0 a)^2 \left[I_2 \left(\dot{v}_{xx}^{(i)} + \frac{1}{R_i^2} \dot{v}_{\theta\theta}^{(i)} \right) + I_3 \left(\ddot{\psi}_{\theta_{xx}}^{(i)} + \frac{1}{R_i^2} \ddot{\psi}_{\theta_{\theta\theta}}^{(i)} \right) \right]$$

where the differential operators are given in Appendix A.

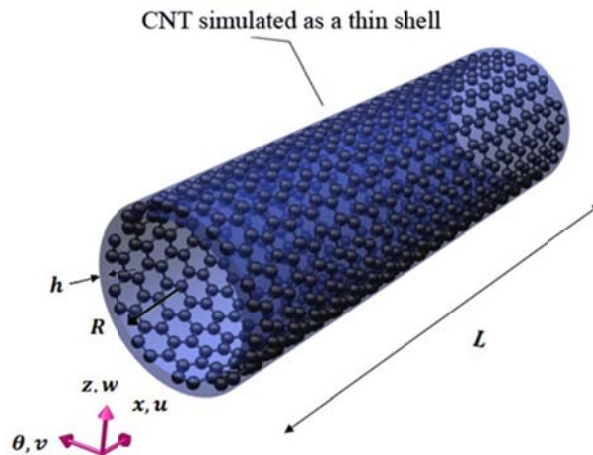


Fig. 1. Schematic of a CNT treated as an elastic shell

For any tube of a DWCNT, different boundary conditions may be considered by the combination of simply-supported (S), clamped (C) and free (F) edges. For example:

Simply-supported-Simply-supported (SS)

$$v = w = \psi_\theta = M_x = N_x = 0, \quad \text{at edges } x = 0, x = L \quad (10)$$

Clamped-Clamped (CC)

$$u = v = w = \psi_x = \psi_\theta = 0, \quad \text{at edges } x = 0, x = L \quad (11)$$

Clamped-Free (CF)

$$\begin{aligned} u = v = w = \psi_x = \psi_\theta = 0, & \quad \text{at edge } x = 0 \\ N_x = N_{x\theta} = M_x = M_{x\theta} = Q_x = 0, & \quad \text{at edge } x = L \end{aligned} \quad (12)$$

3. SOLUTION

a) Radial point interpolation method

In the radial point interpolation method (RPIM), the trial function is given by [18]

$$u^h(x, x_Q) = \sum_{s=1}^n R_s(x) a_s(x_Q) \quad (13a)$$

$$a_s^T(x_Q) = [a_1, a_2, \dots, a_n] \quad (13b)$$

$$R_s^T(x) = [R_1(x), R_2(x), \dots, R_n(x)] \quad (13c)$$

where n is the number of nodes in the neighborhood of a given point x_Q , $R_s(x)$ are radial basis functions in the space coordinates x^T and $a_s(x_Q)$ is the coefficient corresponding to the given point x_Q . The vector of coefficients a can be determined by enforcing Eq. (13) to pass through all the n nodes within the support domain of point x_Q

$$u_s = R_s^T(x)a \quad (s = 1, 2, \dots, n) \quad (14)$$

or in matrix form

$$U_s = R_s a \quad (15)$$

in which $U_s^T = [u_1, u_2, \dots, u_n]$ and R_s is called the moment matrix given by

$$R_s = \begin{bmatrix} R_1(x_1) & R_2(x_1) & \dots & R_n(x_1) \\ R_1(x_2) & R_2(x_2) & \dots & R_n(x_2) \\ \vdots & \vdots & \ddots & \vdots \\ R_1(x_n) & R_2(x_n) & \dots & R_n(x_n) \end{bmatrix} \quad (16)$$

From Eq. (15), one can have

$$a = R_s^{-1} U_s \quad (17)$$

Substituting Eq. (17) into Eq. (13) gives

$$u^h(x) = \sum_{s=1}^n \phi_s(x) u_s \quad (18)$$

in which

$$\phi_s(x) = R_s^T(x) R_s^{-1} \quad (19)$$

The l th derivative of the RPIM shape functions is readily obtained by

$$\phi_s^{(l)}(x) = \left[R_s^{T(l)}(x) \right]^T R_s^{-1} \quad (20)$$

b) RPIDQ analog of field equations

The modal displacement functions for the i th tube are taken as

$$u^{(i)}(x, \theta) = U^{(i)}(x) \cos(m\theta) e^{j\omega t} \quad (21a)$$

$$v^{(i)}(x, \theta) = V^{(i)}(x) \sin(m\theta) e^{j\omega t} \quad (21b)$$

$$w^{(i)}(x, \theta) = W^{(i)}(x) \cos(m\theta) e^{j\omega t} \quad (21c)$$

$$\psi_x^{(i)}(x, \theta) = \Psi_x^{(i)}(x) \cos(m\theta) e^{j\omega t} \quad (21d)$$

$$\psi_\theta^{(i)}(x, \theta) = \Psi_\theta^{(i)}(x) \sin(m\theta) e^{j\omega t} \quad (21e)$$

Substituting these modal functions into the field equations of the DWCNT and discretizing them at the r th given point using the RPIDQ approximation give

$$\begin{aligned} \sum_{s=1}^n \left(L_{11}^{(i)} U_s^{(i)} + L_{12}^{(i)} V_s^{(i)} + L_{13}^{(i)} W_s^{(i)} + L_{14}^{(i)} \Psi_{x_s}^{(i)} + L_{15}^{(i)} \Psi_{\theta_s}^{(i)} \right) \\ = -\omega^2 (1 - (e_0 a)^2 \nabla^2) \left(I_1 \sum_{s=1}^n \phi_{rs} U_s^{(i)} + I_2 \sum_{s=1}^n \phi_{rs} \Psi_{x_s}^{(i)} \right) \end{aligned} \quad (22a)$$

$$\begin{aligned} \sum_{s=1}^n \left(L_{21}^{(i)} U_s^{(i)} + L_{22}^{(i)} V_s^{(i)} + L_{23}^{(i)} W_s^{(i)} + L_{24}^{(i)} \Psi_{x_s}^{(i)} + L_{25}^{(i)} \Psi_{\theta_s}^{(i)} \right) \\ = -\omega^2 (1 - (e_0 a)^2 \nabla^2) \left(I_1 \sum_{s=1}^n \phi_{rs} V_s^{(i)} + I_2 \sum_{s=1}^n \phi_{rs} \Psi_{\theta_s}^{(i)} \right) \end{aligned} \quad (22b)$$

$$\begin{aligned} \sum_{s=1}^n \left(L_{31}^{(i)} U_s^{(i)} + L_{32}^{(i)} V_s^{(i)} + L_{33}^{(i)} W_s^{(i)} + L_{34}^{(i)} \Psi_{x_s}^{(i)} + L_{35}^{(i)} \Psi_{\theta_s}^{(i)} + (1 \right. \\ \left. - (e_0 a)^2 \nabla^2) \left[\sum_{i=2}^N c_{ii} W_s^{(i)} \phi_{rs} - \sum_{i=2}^N c_{ii} W_s^{(i)} \phi_{rs} \right] \right) \\ = -\omega^2 (1 - (e_0 a)^2 \nabla^2) \left(I_1 \sum_{s=1}^n \phi_{rs} W_s^{(i)} \right) \end{aligned} \quad (22c)$$

$$\begin{aligned} \sum_{s=1}^n \left(L_{41}^{(i)} U_s^{(i)} + L_{42}^{(i)} V_s^{(i)} + L_{43}^{(i)} W_s^{(i)} + L_{44}^{(i)} \Psi_{x_s}^{(i)} + L_{45}^{(i)} \Psi_{\theta_s}^{(i)} \right) \\ = -\omega^2 (1 - (e_0 a)^2 \nabla^2) \left(I_2 \sum_{s=1}^n \phi_{rs} U_s^{(i)} + I_3 \sum_{s=1}^n \phi_{rs} \Psi_{x_s}^{(i)} \right) \end{aligned} \quad (22d)$$

$$\delta_b = [X_b^{(1)} \ X_b^{(2)}]^T \quad X_b^{(i)} = [U_b^{(i)} \ V_b^{(i)} \ W_b^{(i)} \ \Psi_{xb}^{(i)} \ \Psi_{\theta b}^{(i)}]^T, \quad (i = 1,2) \quad (28)$$

Using the condensation technique [23], Eq. (26) can be transformed into the standard form of

$$Kg^{-1}(K_{dd} - K_{db}K_{bb}^{-1}K_{bd})\delta_d - \omega^2\delta_d = 0 \quad (29)$$

from which the eigenvalues (ω) can be extracted. The smallest value of ω is the fundamental frequency.

4. RESULTS AND DISCUSSION

The constant values needed for numerical evaluations are $E = 1 \text{ TPa}$, $h = 0.34 \text{ nm}$, $\rho = 2.3 \text{ g/cm}^3$ and $\nu = 0.3$. The configuration of layerwise boundary conditions, for example, will be indicated by (SS/CC), where the pair of SS corresponds to the inner tube and the pair of CC corresponds to the outer tube. Also, for a given inter-tube mode number p , for convenience, the frequency associated with the n th axial and m th circumferential modes will be denoted by $\omega_n^p(m)$. For all the calculations performed in this work, the following radial basis function which is one of the commonest forms with adjustable parameters is employed [18]

$$R_i(x) = \exp\left[-\alpha_c \left(\frac{x-x_i}{d_c}\right)^2\right], \quad \alpha_c = cd_c \quad (30)$$

To define the support domain at a given point, the dimension of the support domain d_s can be determined by $d_s = \alpha_s d_c$, where α_s is the dimensionless size of the support domain and d_c is a characteristic length that relates to the nodal spacing near the point at x_i . For uniformly distributed nodes, d_c is the distance between two neighboring nodes. For non-uniformly distributed nodes, alternatively, d_c can be characterized as an ‘‘average’’ nodal spacing in the support domain of x_i . The physical meaning of the dimensionless size of the support domain α_s is the factor of the average nodal spacing. In one-dimensional cases, an average value of d_c can be computed by $d_c = D_s/(n_{D_s} - 1)$, in which D_s is an estimated support domain, d_s , at the point x_i . It is worth mentioning that D_s should be a reasonably good estimate of d_s and n_{D_s} is the number of nodes that are covered by a known domain with the dimension of D_s . The first three resonant frequencies of a SS/SS DWCNT for up to $n = 19$ regular and irregular grid sampling points are listed in Table 1. This table indicates quite obviously the converging trend of the present numerical solution with increasing number of sampling points for both given radii of support domain.

Table 1. Convergence of resonant frequencies (THz) of a SS/SS DWCNT ($R_1 = 8.5 \text{ nm}$, $L/R_1 = 5$, $\rho = 1.34 \text{ g/cm}^3$, $e_0 a = 0$)

Number of nodes	$\omega_1^1(4)$		$\omega_2^1(5)$		$\omega_3^1(6)$		
	Regular	Irregular	Regular	Irregular	Regular	Irregular	
$\alpha_s = 3$	9	0.1335	0.1338	0.2644	0.2665	0.4096	0.4462
	11	0.1333	0.1334	0.2640	0.2642	0.4017	0.3962
	13	0.1330	0.1331	0.2637	0.2646	0.4002	0.4011
	15	0.1328	0.1330	0.2635	0.2639	0.3998	0.4005
	17	0.1328	0.1328	0.2634	0.2635	0.3997	0.3999
	19	0.1328	0.1328	0.2634	0.2634	0.3997	0.3997
$\alpha_s = 4$	9	0.1334	0.1335	0.2641	0.2652	0.4050	0.4420
	11	0.1332	0.1333	0.2639	0.2640	0.4012	0.4026
	13	0.1329	0.1330	0.2636	0.2638	0.3999	0.4009
	15	0.1328	0.1329	0.2634	0.2637	0.3997	0.4001
	17	0.1328	0.1328	0.2634	0.2634	0.3997	0.3998
	19	0.1328	0.1328	0.2634	0.2634	0.3997	0.3997

To validate the solution procedure presented in this work, the results generated are compared with those of MD simulation reported in [9]. The variation of fundamental frequencies for a SS/SS (5,5) @ (10,10) DWCNT against nanotube aspect ratio is shown in Fig. 2. The nonlocal parameter e_0a needs to be calibrated such that the nonlocal shell model is capable of predicting the results of MD simulation. The calibrated value for e_0a is 1.15 nm. It is observed that there is a good agreement between the results obtained from the nonlocal shell model with its adjusted nonlocal parameter and the ones reported in [9].

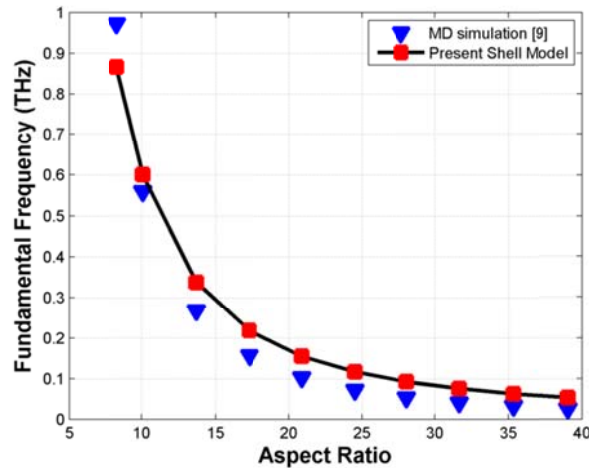


Fig. 2. Fundamental frequencies from the present shell model and MD simulation [9] for a (5,5) @ (10,10) DWCNT under SS/SS boundary conditions

To investigate the effects of nonlocal parameter and aspect ratio on the frequencies of DWCNTs, the variation of nonlocal to local frequency ratio against e_0a for different values of aspect ratio is illustrated in Fig. 3. This figure shows that as the nonlocal parameter increases, the frequency obtained for the nonlocal shell model becomes smaller than that of its local counterpart. It physically means that the small scale effects in the nonlocal model make DWCNT more flexible. Also, it is observed that the effect of e_0a is more pronounced for lower values of aspect ratio. The effect of boundary conditions on the frequency ratio is also studied in Fig. 4. As shown in this figure, as the nonlocal parameter increases, the difference between the boundary conditions increases. According to this figure, the significance of the nonlocal parameter is affected by the type of boundary conditions, so that the nonlocal influence is more prominent for stiffer boundary conditions.

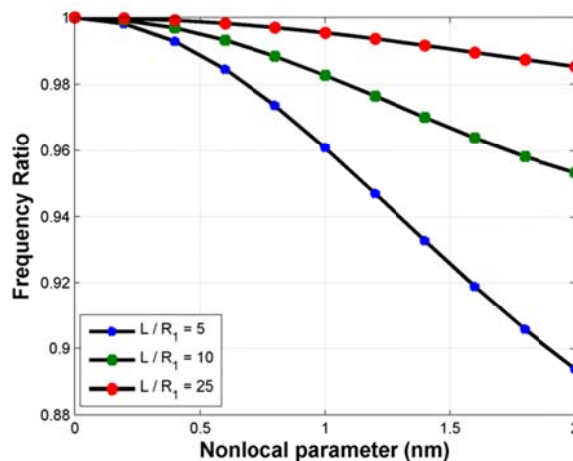


Fig. 3. Variation of frequency ratio versus nonlocal parameter for a SS/CC DWCNT with different values of aspect ratio ($R_1 = 10 \text{ nm}$)

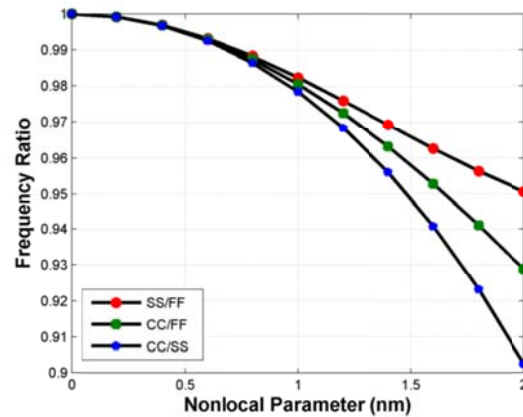


Fig. 4. Variation of frequency ratio versus nonlocal parameter for a DWCNTs with different types of layerwise boundary conditions ($L/R_1 = 10$)

Now, a comparison is made between the results generated by the present shell model and the ones obtained using beam model. To this aim, the results of the present nonlocal Donnell shell model and those of local beam model reported in [7] and also the ones obtained from the nonlocal beam model given in Appendix B for SS/SS DWCNTs are presented in Fig. 5. Different boundary conditions including layerwise end conditions such as FF/CC and SS/CC are considered in these figures. Presented graphically in Figs. 5a and b are the local and nonlocal ($e_0 a = 0.5 \text{ nm}$) fundamental frequencies of a SS/SS DWCNT against the length of nanotube, respectively. For the beam model, the frequencies given by Eq. (B.8) are used in these figures. It can be seen that the fundamental frequency decreases as the length increases. Furthermore, it is found that the beam model tends to overestimate the frequencies of DWCNT so that the discrepancy between the beam and shell models becomes more pronounced for DWCNTs of low length values. Also, it is observed that the nonlocal effect is more prominent in the shell model than that in the beam model. Figs. 5c and d show the fundamental frequencies of DWCNTs with two different layerwise boundary conditions, namely FF/CC and SS/CC. These figures also provide a comparison between the present local Donnell shell model and the local beam model developed in [7]. The difference between beam and shell models for shorter DWCNTs can also be seen in these figures similar to that shown in Figs. 5a and b. Thus, one may conclude that depending on the length of nanotube, the beam model leads to inaccurate results for vibrations of DWCNTs. The reason here is that, the beam model does not take the circumferential mode into account. It should be noted that as the length of nanotube increases, the frequency curves corresponding to the beam and shell models tend to converge. This reveals that the sufficiently long DWCNTs behave like a beam.

Figure 6 depicts the vibrational mode shapes of a SS/SS DWCNT for two different inner radii on the basis of beam model developed in Appendix B. This figure shows two vibrational mode shapes predicted via the beam model corresponding to coaxial and non-coaxial modes. To show the ability of the shell model in predicting new inter-tube resonant frequencies and the related non-coaxial vibrational modes, mode shapes predicted by the shell model are also shown in Fig. 7. As revealed in this figure, further non-coaxial vibrational modes such as ω_1^2 and ω_1^9 for radius $R_1 = 1 \text{ nm}$ and ω_1^4 and ω_1^9 for radius $R_1 = 2 \text{ nm}$ are predictable. Hence, unlike the beam model which is capable of predicting only two inter-tube vibrational modes, the application of the present shell model leads to predict further inter-tube vibrational modes and the associated non-coaxial vibrational modes. Furthermore, non-coaxial vibrational modes may shift to the ones related to higher circumferential mode numbers as the inner radius of DWCNT is increased.

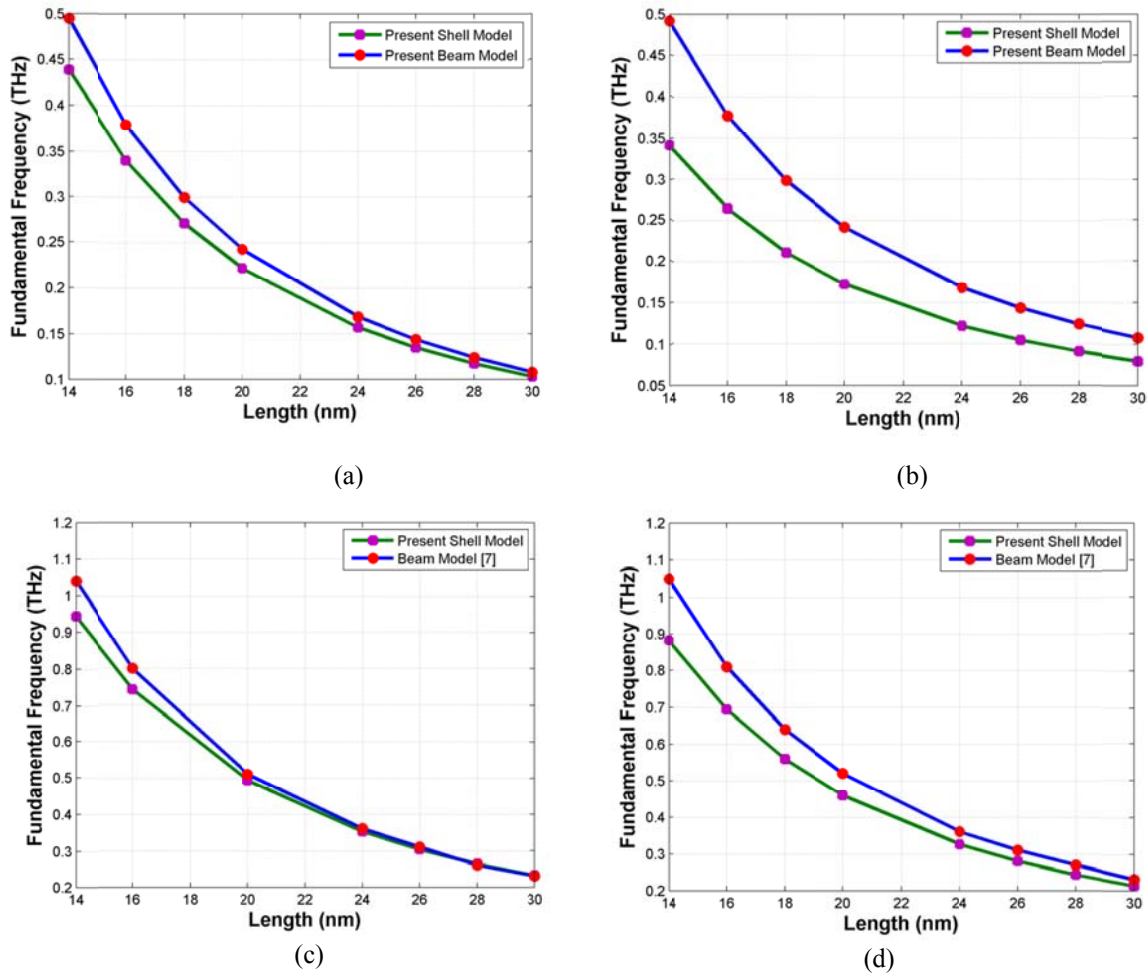


Fig. 5. Comparison between the fundamental frequencies of shell and beam models for a SS/SS DWCNT ($R_1 = 0.35 \text{ nm}$)

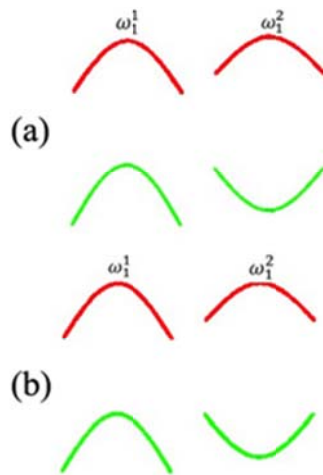


Fig. 6. Mode shapes of a SS/SS DWCNT predicted by the beam model developed in Appendix B: a) with $R_1 = 1 \text{ nm}$ and $L/R_1 = 10$ b) with $R_1 = 2 \text{ nm}$ and $L/R_1 = 10$

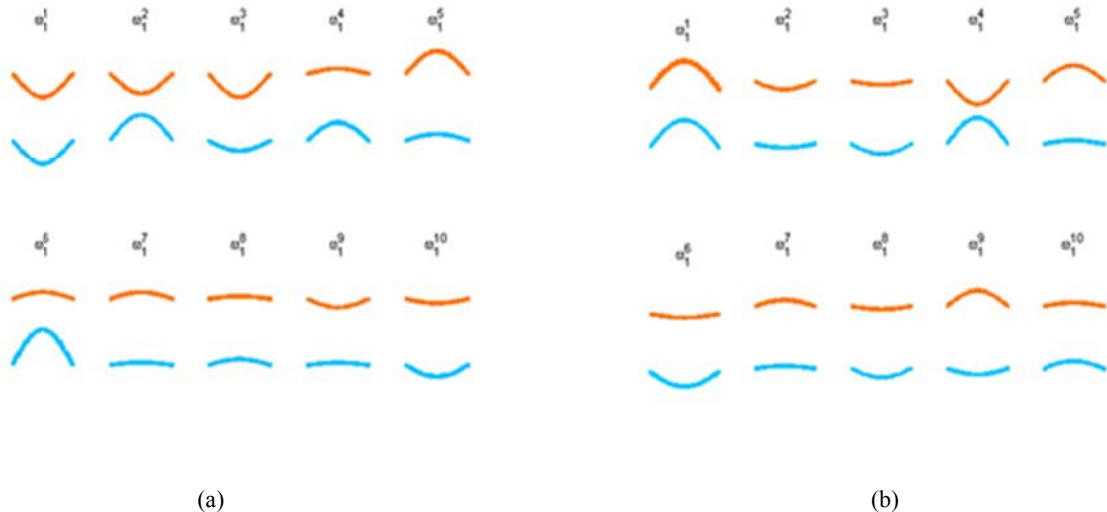


Fig. 7. Mode shapes of a SS/SS DWCNT predicted by the shell model: a) with $R_1 = 1$ nm and $L/R_1 = 10$ b) with $R_1 = 2$ nm $L/R_1 = 10$

5. CONCLUDING REMARKS

The free vibration of DWCNTs with different layerwise boundary conditions was investigated in this work. To this end, a nonlocal Donnell shell model was developed which accounts for the scale effect. The set of governing equations were then numerically solved via the radial point interpolation approximation combined with the GDQ method. Good agreement was observed between the calculated frequencies by the nonlocal shell model and MD simulation. It was indicated that applying the local Donnell shell model leads to overestimated results and one must recourse to the nonlocal version to reduce the relative error. Through comparison between the results generated by the shell model and the ones obtained from the beam model, it was concluded that the beam model tends to overestimate the resonant frequencies of DWCNTs as compared to the shell model, due to not incorporating circumferential mode number into the model. By the present Donnell shell model some new non-coaxial inter-tube resonances of DWCNTs were predicted. Additionally, a shift in non-coaxial modes, which is unpredictable by the beam model, is observed to likely happen when the radius of DWCNTs is varied.

REFERENCES

1. Iijima, S. (1991). Helical microtubes of graphitic carbon. *Nature*, Vol. 8, pp. 354-356.
2. Elishakoff, I. et al. (2012). *Carbon nanotubes and nanosensors: Vibration, buckling and ballistic impact*. ISTE-Wiley, London.
3. Bandow, S., Takizawa, M., Hirahara, K., Yudasaka, M. & Iijima, S. (2001). Raman Scattering Study of Double-Wall Carbon Nanotubes Derived from the Chains of Fullerenes in Single-Wall Carbon Nanotubes. *Chem. Phys. Lett.*, Vol. 337, pp. 48-54.
4. Eringen, A. C. (1983). On differential equations of nonlocal elasticity and solutions of screw dislocation and surface waves. *J. Appl. Phys.*, Vol. 54, pp. 4703-4710.
5. Eringen, A. C. (2002). *Nonlocal continuum field theories*. New York, Springer-Verlag.
6. Li, R. & Kardomateas, G. A. (2007). Vibration characteristics of multiwalled carbon nanotubes embedded in elastic media by a nonlocal elastic shell model. *ASME J. Appl. Mech.*, Vol. 74, pp. 1087-1094.
7. Xu, K. Y., Aifantis, E. C., and Yan, Y. H., 2008, "Vibrations of double-walled carbon nanotubes with different boundary conditions between inner and outer tubes. *ASME J. Appl. Mech.*, Vol. 75, p. 021013.

8. Arash, B. & Ansari, R. (2010). Evaluation of nonlocal parameter in the vibrations of single-walled carbon nanotubes with initial strain. *Physica E*, Vol. 42, pp. 2058-2064.
9. Ansari, R., Rouhi, H. & Sahmani, S. (2011). Calibration of the analytical nonlocal shell model for vibrations of double-walled carbon nanotubes with arbitrary boundary conditions using molecular dynamics. *Int. J. Mech. Sci.*, Vol. 53, pp. 786-792.
10. Ansari, R. & Rouhi, H. (2012). Analytical treatment of the free vibration of single-walled carbon nanotubes based on the nonlocal Flugge shell theory. *ASME J. Eng. Mater. Technol.*, Vol. 134, p. 011008.
11. Ghavanloo, E. & Fazelzadeh, S. A. (2012). Vibration characteristics of single-walled carbon nanotubes based on an anisotropic elastic shell model including chirality effect. *Appl. Math. Model*, Vol. 36, pp. 4988-5000.
12. Yan, Y., Wang, W. & Zhang, L. (2012). Free vibration of the fluid-filled single-walled carbon nanotube based on a double shell-potential flow model. *Appl. Math. Model*, Vol. 36, pp. 6146-6153.
13. Murmu, T., McCarthy, M. A. & Adhikari, S. (2012). Vibration response of double-walled carbon nanotubes subjected to an externally applied longitudinal magnetic field: A nonlocal elasticity approach. *J. Sound Vib.*, Vol. 331, pp. 5069-5086.
14. Hu, Y. G., Liew, K. M. & Wang, Q. (2012). Modeling of vibrations of carbon nanotubes. *Procedia Eng.*, Vol. 31, pp. 343-347.
15. Khosrozadeh, A. & Hajabasi, M. A. (2012) Free vibration of embedded double-walled carbon nanotubes considering nonlinear interlayer van der waals forces. *Appl. Math. Model.*, Vol. 36, pp. 997-1007.
16. Ambrosini, D. & de Borbón, F. (2012). On the influence of the shear deformation and boundary conditions on the transverse vibration of multi-walled carbon nanotubes. *Comput. Mater. Sci.*, Vol. 53, pp. 214-219.
17. Lim, C. W., Li, C. & Yu, J. L. (2012). Free torsional vibration of nanotubes based on nonlocal stress theory. *J. Sound Vib.*, Vol. 331, pp. 2798-2808.
18. Liu, G. R. (2003). *Mesh free methods moving beyond the finite element method*. CRC PRESS.
19. Bellman, R. E., Kashef, B. G. & Casti, J. (1972). Differential quadrature: a technique for rapid solution of nonlinear partial differential equations. *J. Comput. Phys.*, Vol. 10, pp. 40-52.
20. Flugge, W. (1960). *Stresses in shells*. Springer, Berlin.
21. Darvizeh, M., Ansari, R., Darvizeh, A. & Sharma, C. B. (2003). Buckling of fibrous composite cylindrical shells with non-constant radius subjected to different types of loading. *Iran. J. Sci. Technol. Trans. B Eng.*, Vol. 27, pp. 535-550.
22. Donnell, L. H. (1976). *Beam, plates and shells*. New York: McGraw-Hill.
23. Bathe, K. J. (1996). *Finite element procedures*. Englewood Cliffs, NJ Prentice Hall.

APPENDIX A

Differential operators:

$$\begin{aligned}
 l_{11}^{(i)} &= \frac{Eh}{1-\nu^2} \frac{\partial^2}{\partial x^2} + \frac{1}{2} \frac{Eh}{2(1+\nu)} \left(\frac{1}{R_i}\right)^2 \frac{\partial^2}{\partial \theta^2} & l_{12}^{(i)} &= \left(\frac{\nu Eh}{1-\nu^2} + \frac{1}{2} \frac{Eh}{2(1+\nu)}\right) \left(\frac{1}{R_i}\right) \frac{\partial^2}{\partial x \partial \theta} \\
 l_{13}^{(i)} &= \frac{1}{R_i} \frac{\nu Eh}{1-\nu^2} \frac{\partial}{\partial x} & l_{14}^{(i)} &= l_{15}^{(i)} & l_{21}^{(i)} &= l_{12}^{(i)} & l_{22}^{(i)} &= \frac{1}{2} \frac{Eh}{2(1+\nu)} \frac{\partial^2}{\partial x^2} - \frac{Eh}{1-\nu^2} \left(\frac{1}{R_i}\right)^2 \frac{\partial^2}{\partial \theta^2} - \frac{Gh}{R_i^2} \\
 l_{23}^{(i)} &= -\left(\frac{Eh}{1-\nu^2} + Gh\right) \left(\frac{1}{R_i}\right)^2 \frac{\partial}{\partial \theta} & l_{24}^{(i)} &= 0 & l_{25}^{(i)} &= \frac{Gh}{R_i} & l_{31}^{(i)} &= -l_{13}^{(i)} & l_{32}^{(i)} &= -l_{23}^{(i)} \\
 l_{33}^{(i)} &= Gh \frac{\partial^2}{\partial x^2} - Gh \left(\frac{1}{R_i}\right)^2 \frac{\partial^2}{\partial \theta^2} & l_{34}^{(i)} &= Gh \frac{\partial}{\partial x} & l_{35}^{(i)} &= \frac{1}{R_i} Gh \frac{\partial}{\partial \theta} & l_{41}^{(i)} &= l_{42}^{(i)} & l_{43}^{(i)} &= -l_{34}^{(i)} \\
 & & & & & & & = 0 & & \\
 & & & & & & & & & -\left(\frac{1}{R_i}\right)^2 \frac{Eh}{1-\nu^2}
 \end{aligned}$$

$$l_{44}^{(i)} = D \frac{\partial^2}{\partial x^2} + \frac{1(1-\nu)D}{2} \left(\frac{1}{R_i}\right)^2 \frac{\partial^2}{\partial \theta^2} - Gh \quad l_{45}^{(i)} = \left(\nu D + \frac{1(1-\nu)D}{2} \right) \left(\frac{1}{R_i}\right) \frac{\partial^2}{\partial x \partial \theta} \quad l_{51}^{(i)} = 0 \quad l_{52}^{(i)} = l_{25}^{(i)}$$

$$l_{53}^{(i)} = l_{35}^{(i)} \quad l_{54}^{(i)} = l_{45}^{(i)} \quad l_{55}^{(i)} = \frac{1(1-\nu)D}{2} \frac{\partial^2}{\partial x^2} + D \left(\frac{1}{R_i}\right)^2 \frac{\partial^2}{\partial \theta^2} - Gh$$

Algebraic operators:

$$L_{11}^{(i)} = \frac{Eh}{1-\nu^2} \phi_{rs}^{(2)} + \frac{1}{2} \frac{Eh}{2(1+\nu)} \left(\frac{m}{R_i}\right)^2 \quad L_{12}^{(i)} = \left(\frac{\nu Eh}{1-\nu^2} + \frac{1}{2} \frac{Eh}{2(1+\nu)} \right) \phi_{rs}^{(1)} \left(\frac{m}{R_i}\right) \quad L_{13}^{(i)} = \frac{1}{R_i} \frac{\nu Eh}{1-\nu^2} \phi_{rs}^{(1)}$$

$$L_{14}^{(i)} = L_{15}^{(i)} = 0 \quad L_{21}^{(i)} = L_{12}^{(i)} \quad L_{22}^{(i)} = \frac{1}{2} \frac{Eh}{2(1+\nu)} \phi_{rs}^{(2)} - \frac{Eh}{1-\nu^2} \left(\frac{m}{R_i}\right)^2 - \frac{Gh}{R_i^2} \quad L_{23}^{(i)} = - \left(\frac{Eh}{1-\nu^2} + Gh \right) \frac{m}{R_i^2} \quad L_{24}^{(i)} = 0$$

$$L_{25}^{(i)} = \frac{Gh}{R_i} \quad L_{31}^{(i)} = L_{13}^{(i)} \quad L_{32}^{(i)} = L_{23}^{(i)}$$

$$L_{33}^{(i)} = Gh \phi_{rs}^{(2)} - Gh \left(\frac{m}{R_i}\right)^2 - \frac{1}{R^2} \frac{Eh}{1-\nu^2} \quad L_{34}^{(i)} = Gh \phi_{rs}^{(1)} \quad L_{35}^{(i)} = Gh \left(\frac{m}{R_i}\right)$$

$$L_{41}^{(i)} = L_{42}^{(i)} = 0 \quad L_{43}^{(i)} = L_{34}^{(i)} \quad L_{44}^{(i)} = D \phi_{rs}^{(2)} - \frac{1(1-\nu)D}{2} \left(\frac{m}{R_i}\right)^2 - Gh \quad L_{45}^{(i)} = \left(\nu D + \frac{1(1-\nu)D}{2} \right) \left(\frac{m}{R_i}\right) \phi_{rs}^{(1)} \quad L_{51}^{(i)} = 0$$

$$L_{52}^{(i)} = L_{25}^{(i)} \quad L_{53}^{(i)} = L_{35}^{(i)} \quad L_{54}^{(i)} = L_{45}^{(i)}$$

$$L_{55}^{(i)} = \frac{1(1-\nu)D}{2} \phi_{rs}^{(2)} + D \left(\frac{m}{R_i}\right)^2 - Gh$$

APPENDIX B: EXACT SOLUTION FOR THE NONLOCAL BEAM MODEL

$$w_i = \mathcal{W}_i \sin\left(\frac{n\pi x}{L}\right) e^{j\omega t}, \quad (i = 1,2) \tag{B.1}$$

$$EI_1 \frac{\partial^4 w_1}{\partial x^4} + \rho A_1 [1 - (e_0 a)^2 \nabla^2] \frac{\partial^2 w_1}{\partial t^2} - c_{12} [1 - (e_0 a)^2 \nabla^2] (w_1 - w_2) = 0$$

$$EI_2 \frac{\partial^4 w_2}{\partial x^4} + \rho A_2 [1 - (e_0 a)^2 \nabla^2] \frac{\partial^2 w_2}{\partial t^2} - c_{21} [1 - (e_0 a)^2 \nabla^2] (w_2 - w_1) = 0 \tag{B.2}$$

Substituting Eq. (B.1) into Eq. (B.2) gives the following algebraic equations

$$\left(EI_1 \left(\frac{n\pi}{L}\right)^4 - \rho A_1 \omega^2 \left[1 - (e_0 a)^2 \left(\frac{n\pi}{L}\right)^2 \right] - c_{12} \left[1 + (e_0 a)^2 \left(\frac{n\pi}{L}\right)^2 \right] \right) \mathcal{W}_1 + c_{12} \left[1 + (e_0 a)^2 \left(\frac{n\pi}{L}\right)^2 \right] \mathcal{W}_2 = 0$$

$$\left(EI_2 \left(\frac{n\pi}{L}\right)^4 - \rho A_2 \omega^2 \left[1 - (e_0 a)^2 \left(\frac{n\pi}{L}\right)^2 \right] - c_{21} \left[1 + (e_0 a)^2 \left(\frac{n\pi}{L}\right)^2 \right] \right) \mathcal{W}_2 + c_{21} \left[1 + (e_0 a)^2 \left(\frac{n\pi}{L}\right)^2 \right] \mathcal{W}_1 = 0$$

$$(K - \omega^2 M) \{ \mathcal{W} \} = \{ 0 \} \tag{B.3}$$

$$\tag{B.4}$$

where

$$K = \begin{bmatrix} EI_1 \left(\frac{n\pi}{L}\right)^4 - c_{12} \left[1 + (e_0 a)^2 \left(\frac{n\pi}{L}\right)^2 \right] & c_{12} \left[1 + (e_0 a)^2 \left(\frac{n\pi}{L}\right)^2 \right] \\ c_{21} \left[1 + (e_0 a)^2 \left(\frac{n\pi}{L}\right)^2 \right] & EI_2 \left(\frac{n\pi}{L}\right)^4 - c_{21} \left[1 + (e_0 a)^2 \left(\frac{n\pi}{L}\right)^2 \right] \end{bmatrix} \tag{B.5}$$

$$M = \begin{bmatrix} \rho A_1 \left[1 - (e_0 a)^2 \left(\frac{n\pi}{L}\right)^2 \right] & 0 \\ 0 & \rho A_2 \left[1 - (e_0 a)^2 \left(\frac{n\pi}{L}\right)^2 \right] \end{bmatrix} \tag{B.6}$$

$$\mathcal{W} = \begin{Bmatrix} \mathcal{W}_1 \\ \mathcal{W}_2 \end{Bmatrix} \quad (\text{B.7})$$

The nontrivial solution of (B.4) gives $\det(K - \omega^2 M) = 0$. The following explicit formula for the resonant frequencies of the DWCNT can be obtained as

$$\omega = \frac{\sqrt{2}}{2} \sqrt{\frac{K_{11}M_{22} + M_{11}K_{22} \pm \sqrt{(K_{22}M_{11} - K_{11}M_{22})^2 + 4M_{11}M_{22}K_{12}K_{21}}}{M_{11}M_{22}}} \quad (\text{B.8})$$

where

$$\begin{aligned} K_{11} &= EI_1 \left(\frac{n\pi}{L}\right)^4 - c_{12} \left[1 + (e_0 a)^2 \left(\frac{n\pi}{L}\right)^2 \right] & K_{22} &= EI_2 \left(\frac{n\pi}{L}\right)^4 - c_{21} \left[1 + (e_0 a)^2 \left(\frac{n\pi}{L}\right)^2 \right] & K_{12} &= c_{12} \left[1 + (e_0 a)^2 \left(\frac{n\pi}{L}\right)^2 \right] \\ K_{21} &= c_{21} \left[1 + (e_0 a)^2 \left(\frac{n\pi}{L}\right)^2 \right] & M_{11} &= \rho A_1 \left[1 - (e_0 a)^2 \left(\frac{n\pi}{L}\right)^2 \right] & M_{22} &= \rho A_2 \left[1 - (e_0 a)^2 \left(\frac{n\pi}{L}\right)^2 \right] \end{aligned}$$